Available online at www.sciencedirect.com

SciVerse ScienceDirect

Ceramics International 39 (2013) 1477–1483

CERAMICS INTERNATIONAL

www.elsevier.com/locate/ceramint

An innovative fabrication of nano-HA coatings on Ti-CaP nanocomposite layer using a combination of friction stir processing and electrophoretic deposition

Hamidreza Farnoush[a,*], Ali Sadeghi[b], Ashkan Abdi Bastami[a], Fathollah Moztarzadeh[b], Jamshid Aghazadeh Mohandesi[a]

[a]*Department of Mining and Metallurgical Engineering, Amirkabir University of Technology, P.O. Box 15875-4413, Tehran, Iran*
[b]*Biomedical Engineering Department, Amirkabir University of Technology, P.O. Box 15875-4413, Tehran, Iran*

Received 20 June 2012; received in revised form 26 July 2012; accepted 27 July 2012
Available online 4 August 2012

Abstract

In the present study, a combination of friction stir processing and electrophoretic deposition was used to fabricate nano-hydroxyapatite coatings on the Ti-CaP nanocomposite surface layer. A constant tool rotation rate of 250 rpm, travel speed of 16 mm/min and plunge depth of 1.2 mm with a tool tilt angle of 3° were used to incorporate nano-hydroxyapatite particles into Ti–6Al–4V substrates. Microstructure of the stir zone was analyzed using optical and scanning electron microscopy. Microhardness profile and AFM analysis of substrates were then studied. The electrophoretic deposition of nano-HA particles was carried out at constant voltage of 30 V after 60 s. The as-deposited nano-HA coating was characterized employing scanning electron microscope and X-ray diffraction. The results of adhesion test and potentiodynamic polarization measurements showed that Ti-CaP nanocomposite layer could effectively increase the bonding strength between coating and substrate as well as corrosion resistance.

Keywords: B. Nanocomposites; D. Apatite; E. Biomedical applications; Electrophoretic deposition

1. Introduction

Ti–6Al-4V (Ti64) is the most widely used titanium alloy for load bearing bioimplant applications [1]. It offers a high strength to weight ratio, low modulus, high biocompatibility and resistance to corrosion [1]. However, due to poor osteoinductive properties of titanium alloys, coating hydroxyapatite ($Ca_{10}(PO_4)_6(OH)_2$) on Ti64 substrates has received considerable attention [2]. Hydroxyapatite (HA), a biocompatible ceramic material with high osseoconductivity, is commonly used as a filler to replace amputated bone or as a coating to promote bone ingrowth into prosthetic implants [2]. However, due to poor mechanical properties of HA, a great deal of interest is focused on improving the mechanical and biological performances by using HA coatings on Ti64 alloy [2]. Electrophoretic deposition (EPD) is successfully implemented for the fabrication of dense and uniform HA coatings on the substrates with various geometries [3–6]. Moreover, EPD is more economically favorable technique among other methods such as plasma spray [7,8], sol–gel [9,10], and biomimetic [11,12]. The basis of an EPD process is the migration of colloidal particles suspended in a liquid medium under the influence of an electric field and their deposition onto an oppositely charged electrode [13].

In order to cope with metallic substrate degradation and HA decomposition, in fabrication of HA coatings on the Ti64 substrates, sintering temperatures is set at < 1000 °C; however, at these temperatures HA densification is insufficient [14]. Furthermore, due to high difference between thermal expansion coefficients (CTE) of Ti64 substrate and HA [15,16], thermal contraction mismatch leads to the cracks formation during cooling the system from the elevated temperatures; additionally, a considerable firing shrinkage during sintering stimulates the propagation of

*Corresponding author. Tel.: +98 21 64542949; fax: +98 21 64542941.
E-mail address: farnoush@aut.ac.ir (H. Farnoush).

0272-8842/$ - see front matter © 2012 Elsevier Ltd and Techna Group S.r.l. All rights reserved.
http://dx.doi.org/10.1016/j.ceramint.2012.07.092

cracks in coatings [17]. One promising way to deal with these problematic issues is the use of inner layers between substrate and HA coating. The inner layers act as a diffusion barrier and reducing the decomposition of the HA powders in the second layer during sintering [16,17]. Additionally, the presence of inner layers in HA coatings improves the bonding strength and reduces CTE mismatch at HA/Ti64 interface [15,16].

Recently, friction stir processing (FSP) has been demonstrated as an effective technique for the fabrication of nanocomposite surface layer enhancing microstructural modification of the working piece [18]. In the FSP, a rotating tool was inserted into a single piece of material, for severe plastic deformation, material mixing, and thermal exposure, resulting in significant microstructural refinement, densification, and homogenization [18]. This technique has been successfully applied in the production of fine grained structures, surface composites, and microstructural modification of castings [18]. FSP is a solid state process which has the advantages of adjusting mechanical properties by optimizing tool design and process parameters and avoiding the excessive interfacial reactions of reinforcement with metal matrix [19]. Since the bonding strength of HA coating is improved by incorporating an inner layer [15–17], FSP can be potentially applied for the modification of electrophoretically deposited nano-HA coatings. To the authors' best knowledge, there is no through work reporting the influence of FSP on the bonding strength of HA coatings.

In the current study, a combination of friction stir processing (FSP) and electrophoretic deposition (EPD) was used to fabricate nano-HA coatings on Ti-CaP nanocomposite layer. The FSP was performed by plunging a rotating, cylindrical tool into the work-piece grooves containing nano-HA powders. Then, the EPD of nano-HA particles on Ti-CaP nanocomposite layer was studied. Finally, the electrochemical corrosion behavior in a simulated body fluid solution and the bonding strength of friction stir processed and as-received samples were discussed. The fabricated Ti-CaP nanocomposite layer and nano-HA coatings were characterized employing microhardness measurements, SEM, XRD, and AFM analyses.

2. Experimental procedures

2.1. Friction stir processing on Ti–6Al–4V substrates

Ti–6Al–4V mill-annealed plates and nano-sized HA powders (synthesized by precipitation method [3]) were used as substrate and reinforcement particulates, respectively. The as-received substrates (AR) was 3-mm-thick mill-annealed Ti–6Al–4V plates with the chemical composition of Al=6.28, V=4.90, Fe=0.29, Nb=0.05, Mn=0.03. Cr=0.02, Si=0.05, Sn < 0.05, Mo < 0.03, Cu < 0.02, Zr=0.01, and Ti balance (all in wt%). The as-received plates were additionally annealed at 850 °C for 1.5 h to form a homogenous microstructure with equiaxed grains. The whole surface of a 10 cm × 2 cm work piece was subjected to friction stir processing (FSP). The used tungsten carbide tool was 16 mm in diameter and the tilt angle was 3°. The tool rotation was set to be 250 rpm, plunge depth was 1.5 mm and its advancing speed was 16 mm/min. Three grooves with 1 mm depth and 2 mm width were machined on the surface of work piece and separated from each other by a 2 mm distance. Subsequently, nano-sized HA powders were compacted into the grooves and 3 passes FSP was carried out on the prepared sheets under an argon gas shrouding system. Cross and lateral sections of the friction stir processed sample (designated as Ti-CaP) was mounted, and then mechanically polished, followed by etching in an etchant composed of 2.5% HNO_3, 1.5% HF, and 96% distilled water. The phase composition of Ti-CaP sample was analyzed by XRD (Philips PW 1480) in $2\theta = 20–100^\circ$ range at a step size of 0.02° and a count time of 0.6 s. The hardness profile was obtained using a scanning microhardness tester with a load of 100 g and a dwell time of 10 s. Five Vickers hardness indentations were performed on each specimen. Surface topography and roughness of Ti-CaP sample were characterized by scanning probe microscope (SPM, DME DS-95-50E). The microstructural characterization and elemental composition of the Ti-CaP sample were analyzed by using scanning electron microscope (SEM, Philips XL 30) equipped with an Energy Dispersive Spectrometer (EDS).

2.2. Electrophoretic deposition of nano-HA powders

Nanocrystalline hydroxyapatite powders (synthesized by precipitation method [3]) were used as the coating material. The suspension was prepared by adding 1 g of HA powders into 50 mL of absolute ethanol (Merck, USA). The addition of 1 g/L iodine (dispersant) to ethanol was resulted in positively charged particles. The prepared suspension was dispersed in a 50 kHz ultrasonic bath for 60 min, and then was immediately used for electrophoretic deposition (EPD) without further aging. Ti–6Al–4V substrate as the working electrode and 316 L stainless steel as the counter electrode were immersed in the suspension with a fixed distance of 10 mm. Prior to deposition, Ti–6Al–4V substrates were ground with 400–1200 grit SiC papers, then washed out with detergent and degreased with acetone, and finally passivated in a HF (100 mL/L)–HNO_3 (300 mL/L) solution. One side of the cathode was masked with a non-conducting tape. The surface area of the cathode was 1 cm^2. The EPD process was conducted on the Ti-CaP nanocomposite layer for 60 s under a constant voltage of 30 V. After deposition, the green coatings were dried in air for 24 h at room temperature. Sintering of the coatings was carried out in an argon-purged atmosphere at 900 °C. The heating rate and cooling rate were the same (10 °C/min) and the dwell time was 1.5 h. The phase composition of coated surface was analyzed by XRD (Philips PW 1480), by scanning in $2\theta = 20–100^\circ$ range at a step size of 0.02° and a count time of 0.6 s. The microstructural characterization of the as-deposited sample (designated as HA/Ti-CaP)

Table 1
Chemical composition of simulated body fluid employed in this study.

Ion	SBF (mM)	Blood plasma (mM)
Na^+	142.0	142.0
K^+	5.0	5.0
Mg_2^+	1.5	1.5
Ca_2^+	2.5	2.5
Cl^-	147.8	103.0
HCO_3^-	4.2	27.0
HPO_4^{2-}	1.0	1.0
SO_4^{2-}	0.5	0.5

was carried out by using SEM (Philips XL 30). To investigate electrochemical corrosion behavior of HA/Ti-CaP coating, samples were embedded in cold-curing epoxy resin, exposing a surface area of 1 cm^2. Potentiodynamic polarization test in a corrected-SBF solution [20], open to air at 37 °C and at the physiological pH 7.40, was performed using AutoLab PGstat 30. The chemical composition of the employed SBF is given in Table 1. All potentials were measured with respect to a saturated calomel electrode. Two parallel graphite rods served as the counter electrode for current measurement. From the polarization curve, the corrosion parameters were evaluated by Tafel extrapolation method by Nova v1.6 software. Bonding strengths of the sintered samples were measured by using a pull-off adhesion tester (PosiTest, Defelsko). A 10 mm diameter Al rod was glued onto the coated surface with epoxy resin as the hardener. The adhesive strength was then calculated as the tensile force per fracture area.

3. Results and discussion

3.1. Characterization of Ti-CaP nanocomposite surface layer and HA/Ti-CaP coating

In Fig. 1, the cross section of fabricated Ti-CaP layer exhibits the grain refining within the stir zone. During a sever plastic deformation of Ti64 alloy, the occurrence of dynamic recrystallization (DRX) is the most probable restoration mechanism [21]. The severity of plastic deformation results in the formation of dislocation tangle zones close to the grain boundaries. Then, annihilation of dislocations leads to sub-grain formation and finally new dislocations-free grains are produced with high misorientations [22]. On the other hand, the grain growth was limited effectively due to severe deformation and short time at elevated temperature in FSP zone.

Fig. 2 presents the microhardness profile of Ti-CaP sample versus the distance from the surface. An approximately 33% increase in microhardness can be achieved in severe deformed layer. Besides, the thickness of the friction stir processed layer may reach to 160 μm. The grain refinement accompanied by a considerable increment in hardness is observed due to friction stir processing and the distribution of nano-hydroxyapatite particles along the mentioned depth.

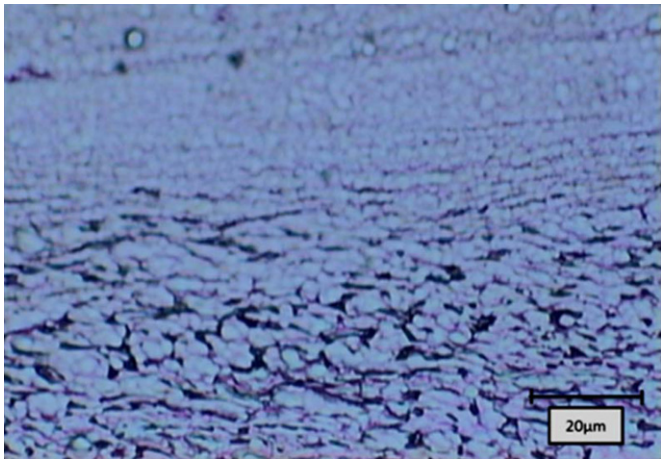

Fig. 1. Cross section of a typical fabricated Ti-CaP layer exhibiting grain refinement in the stir zone.

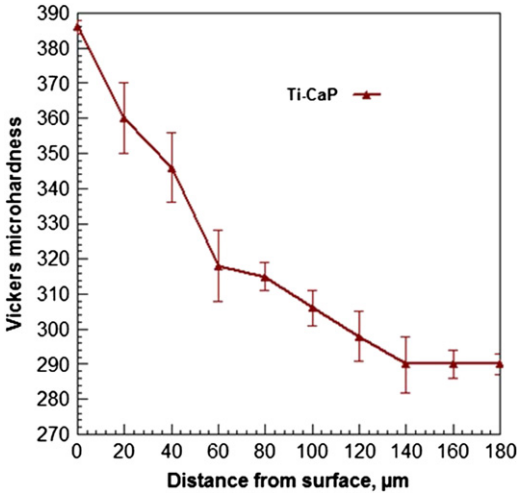

Fig. 2. Vickers microhardness profile versus the distance from surface of Ti-CaP nanocomposite layer.

Typical microstructure of nanocomposite surface layer fabricated by 3 passes FSP is shown in Fig. 3a. Obviously, there are nanoparticles (~50 nm) distributed uniformly in the titanium matrix. The EDS spectrum and quantitative results of the average element composition are shown in Fig. 3b. The Ca/P atomic ratio is 1.21, which concludes that the phase is likely to be between octacalcium phosphate (OCP, $Ca_8(HPO_4)_2(PO_4)_4 \cdot 5H_2O$) with Ca/P=1.3 and dicalcium phosphate anhydrous (DCPA, $CaHPO_4$) with Ca/P=1. It should be noted that the transformation of HA phase to OCP and DCPA phases is affected by FSP parameters which determines the temperature and processing time during severe plastic deformation.

Fig. 4 shows the surface topography of Ti-CaP nanocomposite layer. It is seen that the surface layer is composed of nanoparticles ranging from 40 to 60 nm which is in agreement with Fig. 3a. In addition, the average surface roughness height obtained from roughness analysis

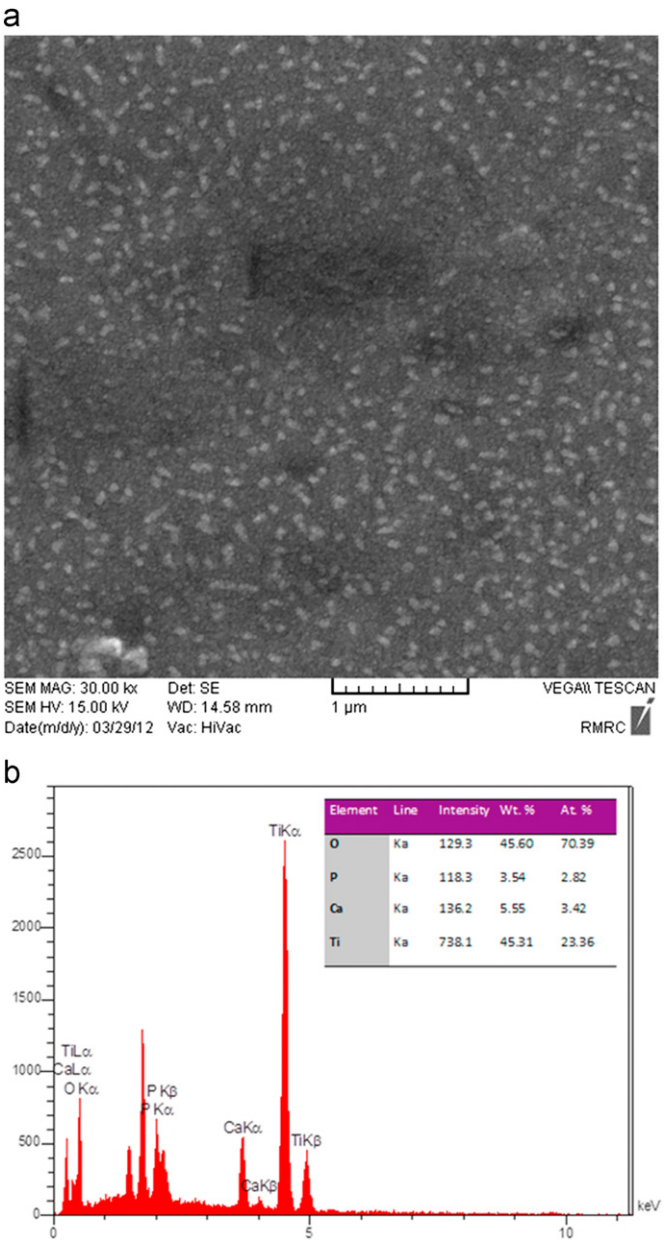

Fig. 3. SEM micrograph (a) and EDS spectrum (b) of fabricated Ti-CaP nanocomposite layer showing CaP particles dispersion within the stir zone.

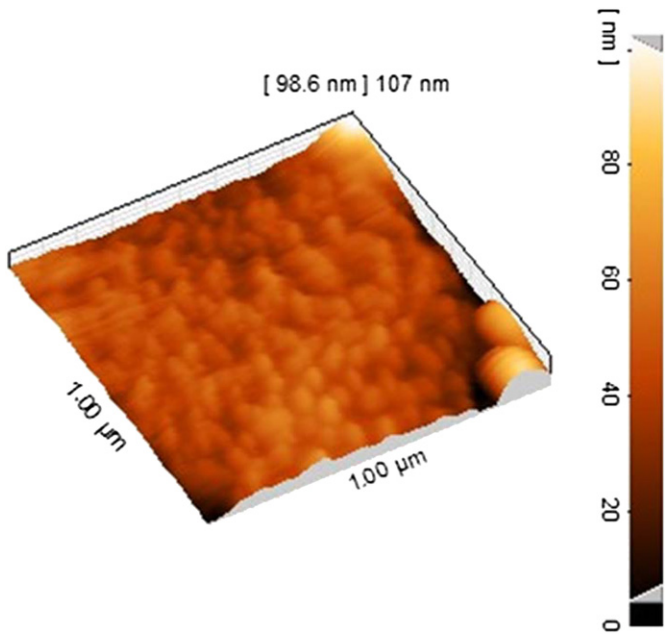

Fig. 4. AFM 3d image of the fabricated Ti-CaP nanocomposite surface layer.

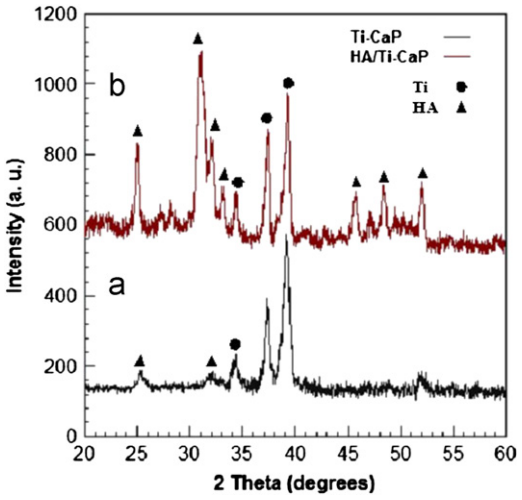

Fig. 5. X-ray diffraction patterns of (a) Ti-CaP substrate and (b) as-deposited HA/Ti-CaP sample.

was 98.6 nm. The characterization of the surface roughness is very important for biomedical application where an appropriate roughened surface is highly desirable due to its higher bonding strength with the coating [23].

Fig. 5 illustrates XRD spectra of Ti-CaP nanocomposite surface layer and as-deposited HA/Ti-CaP sample. The pattern in Fig. 5a reveals a typical fabricated Ti-CaP layer; no titanium oxide reflection was detected using XRD. Reflections related to HA were indicative of its presence in the fabricated composite layers. However, the number of HA reflections and their associated intensities were limited; these are attributed to its relatively low volume fraction in the composite layer. In the spectrum shown in Fig. 5b, the peaks appeared at $2\theta = 25.8^\circ$, 28.7°, 31°, 32.1°, 33.3°, 45.7°, 48.3° and 52° are corresponded to (002), (210), (211), (112), (222) and (321) planes of hydroxyapatite crystal, respectively [24]. Furthermore, the characteristics peaks of Ti at $2\theta = 37.4^\circ$ and 39.3° are apparently distinguishable in both Ti-CaP and HA/Ti-CaP samples which are assigned to (002) and (101) planes, respectively. Also, SEM micrograph of the nano-HA coated on Ti-CaP sample shown in Fig. 6 indicates that the coated surface is composed of HA nanoparticles with the size of ~76 nm.

3.2. Bonding strength and corrosion behavior of HA/Ti-CaP coatings

The mean values of bonding strength for the coated samples are presented in Fig. 7. Compared with the HA/

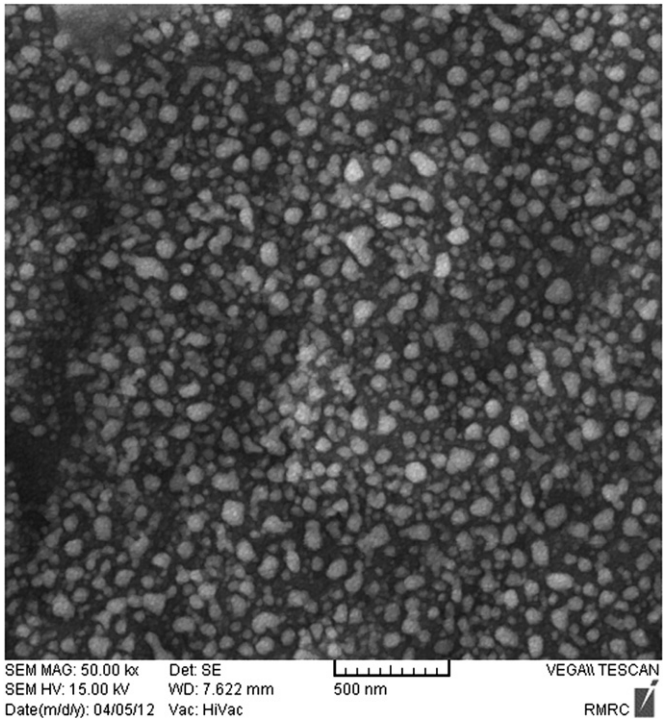

Fig. 6. SEM micrograph showing the surface morphology of as-deposited HA/Ti-CaP sample.

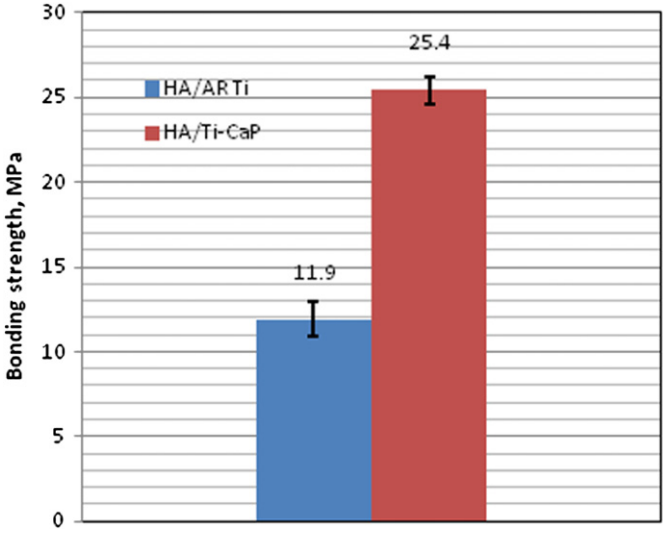

Fig. 7. Bonding strength of HA/AR Ti and HA/Ti-CaP samples.

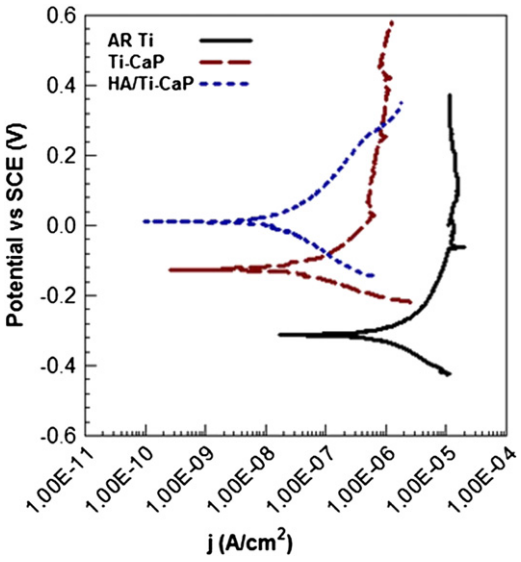

Fig. 8. Potentiodynamic polarization curves of AR Ti, Ti-CaP and HA/Ti-CaP samples in SBF at 37 °C.

AR Ti sample, the bonding strength of HA/Ti-CaP sample is increased by a factor of 2.1 which is higher than those reported for HA coated samples (7–11 MPa) [25]. The enhancement in bonding strength stems from reducing thermal expansion mismatch between Ti64 and the HA coating by introducing Ti-CaP inner layer. Furthermore, the Ti-CaP nanocomposite layer acts as a diffusion barrier and reduces the decomposition of HA coating during sintering. As a result, the dense HA/Ti-CaP coatings with reduced micro-cracks lead to higher bonding strength.

The potentiodynamic polarization curves of the AR Ti, Ti-CaP and HA/Ti-CaP samples in a corrected-SBF solution are depicted in Fig. 8. The corrosion parameters, extracted from polarization curves using Tafel least square fitting method, are listed in Table 2. Additionally, the polarization resistance (Rp) is estimated by the use of Stern–Geary equation ($R_p = (\beta a \times \beta c/2.303(\beta a + \beta c))(1/I_{corr})$) [26]. The results corresponding to HA/Ti-CaP sample imply a significant decrease in the corrosion current density (I_{corr}), and an increase in the corrosion potential (E_{corr}), linear polarization resistance (R_p) and corrosion rate. This indicates that Ti-CaP inner layer helps to produce a coating with fewer micro-cracks. When microcracks are present in the HA coatings, conducting paths between the corrosive medium and the Ti64 substrate will eventually be formed. By implementation of friction stir processing, the Ti-CaP inner layer acts as a barrier to the penetration/transport of chloride ions and water molecules through the coating, transport of ions the coating, and hinders the subsequent electrochemical reactions at the interface of HA and Ti64. In addition, the corrosion rate of Ti-CaP sample is lower as compared with the AR substrate which is caused by rapid formation of stable passive layer due to its fine grained microstructure [27–29]. The reduction of grain size plays an important role in enhancing the activity of electrons at the grain boundaries. In this regard, the surface becomes more electrochemically reactive giving rise to an increase in passivation ability resulting in rapid formation of a mechanically strong and stable passive film [27–29].

4. Conclusions

In the present study, a combination of friction stir processing and electrophoretic deposition was performed to fabricate

Table 2
Electrochemical corrosion parameters of AR Ti, Ti-CaP and HA/Ti-CaP samples.

Sample	E_{corr} (mV)	I_{corr} (μA/cm^2)	β_a (V/decade)	β_c (V/decade)	R_p (Ω cm^2)	Corrosion rate (mm/year) × 10^{-2}
AR Ti	−327	2.76	0.23	0.28	19,925	2.4
Ti-CaP	−127	0.048	0.07	0.12	390,030	0.041
HA/Ti-CaP	0.011	0.021	0.13	0.15	1430,510	0.018

the nano-HA coatings on Ti-CaP nanocomposite surface layer. The FSP was performed at a constant tool rotation rate of 250 rpm, travel speed of 16 mm/min and plunge depth of 1.2 mm with a tool tilt angle of 3°. The microhardness of Ti-CaP nanocomposite layer was reached about 386 HV due to the grain refinement and the distribution of nano-hydroxyapatite particles. The cathodic electrophoretic deposition of nano-HA particles from ethanol based suspension was carried out on Ti-CaP and AR Ti specimens at constant voltage of 30 V after 60 s. It was found that FSP process leads to an improvement in thermal expansion mismatch which could effectively improve the bonding strength between coating and substrate. The electrochemical corrosion behavior of the nano-HA coatings in SBF solution at 37 °C was investigated by means of potentiodynamic polarization test. The results imply that Ti-CaP inner layer significantly decreases the corrosion current density, and increases the corrosion potential, linear polarization resistance and corrosion rate of HA/Ti-CaP sample.

References

[1] M. Geetha, A.K. Singh, R. Asokamani, A.K. Gogia, Ti based biomaterials, the ultimate choice for orthopaedic implants—a review, Progress in Materials Science 54 (2009) 397–425.

[2] S.R. Paital, N.B. Dahotre, Calcium phosphate coatings for bio-implant applications: materials, performance factors, and methodologies, Materials Science and Engineering R 66 (2009) 1–70.

[3] H. Farnoush, J.Aghazadeh Mohandesi, D.Haghshenas Fatmehsari, F. Moztarzadeh, Modification of electrophoretically deposited nano-hydroxyapatite coatings by wire brushing on Ti–6Al–4V substrates, Ceramics International 38 (2012) 4885–4893.

[4] H. Farnoush, J. Aghazadeh Mohandesi, D. Haghshenas Fatmehsari, Effect of particle size on the electrophoretic deposition of hydroxyapatite coatings: a kinetic study based on a statistical analysis, International Journal of Applied Ceramic Technology, http://dx.doi.org/10.1111/j.1744-7402.2012.02818.x, in press.

[5] C. Kaya, Electrophoretic deposition of carbon nanotube-reinforced hydroxyapatite bioactive layers on Ti–6Al–4V alloys for biomedical applications, Ceramics International 34 (2008) 1843–1847.

[6] H. Farnoush, J. Aghazadeh Mohandesi, D. Haghshenas Fatmehsari, F. Moztarzadeh, A kinetic study on the electrophoretic deposition of hydroxyapatite-titania nanocomposite based on a statistical approach, Ceramics International, http://dx.doi.org/10.1016/j.ceramint.2012.05.070, in press.

[7] S. Sathish, M. Geetha, S.T. Aruna, N. Balaji, K.S. Rajam, R. Asokamani, Studies on plasma sprayed bi-layered ceramic coating on bio-medical Ti–13Nb–13Zr alloy, Ceramics International 37 (2011) 1333–1339.

[8] A. Dey, S.K. Nandi, B. Kundu, C. Kumar, P. Mukherjee, S. Roy, A.K. Mukhopadhyay, M.K. Sinha, D. Basu, Evaluation of hydroxyapatite and β-tri calcium phosphate microplasma spray coated pin intra-medullary for bone repair in a rabbit model, Ceramics International 37 (2011) 1377–1391.

[9] I. Sopyan, S. Ramesh, N.A. Nawawi, A. Tampieri, S. Sprio, Effects of manganese doping on properties of sol–gel derived biphasic calcium phosphate ceramics, Ceramics International 37 (2011) 3703–3715.

[10] A. Yelten, S. Yilmaz, F.N. Oktar, Sol–gel derived alumina–hydroxyapatite–tricalcium phosphate porous composite powders, Ceramics International 38 (2012) 2659–2665.

[11] H. Li, Z. Guo, B. Xue, Y. Zhang, W. Huang, Collagen modulating crystallization of apatite in a biomimetic gel system, Ceramics International 37 (2011) 2305–2310.

[12] D. Wei, Y. Zhou, Preparation, biomimetic apatite induction and osteoblast proliferation test of TiO_2-based coatings containing P with a graded structure, Ceramics International 35 (2009) 2343–2350.

[13] A.R. Boccaccini, S. Keim, R. Ma, Y. Li, I. Zhitomirsky, Journal of the Royal Society Interface 7 (2010) S581–S613.

[14] S. Salman, O. Gunduz, S. Yilmaz, M.L. Öveçoğlu, R.L. Snyder, S. Agathopoulos, F.N. Oktar, Sintering effect on mechanical properties of composites of natural hydroxyapatites and titanium, Ceramics International 35 (2009) 2965–2971.

[15] O. Albayrak, O.E. Atwani, S. Altintas, Hydroxyapatite coating on titanium substrate by electrophoretic deposition method: effects of titanium dioxide inner layer on adhesion strength and hydroxyapatite decomposition, Surface and Coatings Technology 202 (2008) 2482–2487.

[16] P.C. Rath, L. Besra, B.P. Singh, S. Bhattacharjee, Titania/hydroxyapatite bi-layer coating on Ti metal by electrophoretic deposition: Characterization and corrosion studies, Ceramics International 38 (2012) 3209–3216.

[17] M. Wei, A.J. Ruys, M.V. Swain, B.K. Milthorpe, C.C. Sorrell, Hydroxyapatite-coated metals: interfacial reactions during sintering, Journal of Materials Science: Materials in Medicine 16 (2005) 101–106.

[18] R.S. Mishra, Z.Y. Ma, Friction stir welding and processing, Materials Science and Engineering R 50 (2005) 1–78.

[19] M. Salehi, M. Saadatmand, J.Aghazadeh Mohandesi, Optimization of process parameters for producing AA6061/SiC nanocomposites by friction stir processing, Transactions of Nonferrous Metals Society of China 22 (2012) 1055–1063.

[20] T. Kokubo, Bioactive glass ceramics: properties and applications, Biomaterials 12 (1991) 155–163.

[21] Z. Guo, A.P. Miodownik, N. Saunders, J.P. Schillé, Influence of stacking-fault energy on high temperature creep of alpha titanium alloys, Scripta Materialia 54 (2006) 2175–2178.

[22] M. Hoseini, M.H. Pourian, F. Bridier, H. Vali, J.A. Szpunar, P. Bocher, Thermal stability and annealing behaviour of ultrafine grained commercially pure titanium, Materials Science and Engineering A 532 (2012) 58–63.

[23] C.Y. Zheng, F.L. Nie, Y.F. Zheng, Y. Cheng, S.C. Weic, R.Z. Valiev, Enhanced in vitro biocompatibility of ultrafine-grained titanium with hierarchical porous surface, Applied Surface Science 257 (2011) 5634–5640.

[24] C.Q. Ning, Y. Zhou, In vitro bioactivity of a biocomposite fabricated from HA and Ti powders by powder metallurgy method, Biomaterials 23 (2002) 2909–2915.

[25] C.T. Kwok, P.K. Wong, F.T. Cheng, H.C. Man, Characterization and corrosion behavior of hydroxyapatite coatings on Ti6Al4V fabricated by electrophoretic deposition, Applied Surface Science 255 (2009) 6736–6744.
[26] M. Stern, A.L. Geary, Electrochemical polarization: I. A theoretical analysis of the shape of polarization curves, Journal of the Electrochemical Society 104 (1957) 56–63.
[27] A. Balyanov, J. Kutnyakova, N.A. Amirkhanova, V.V. Stolyarov, R.Z. Valiev, X.Z. Liao, Y.H. Zhao, Y.B. Jiang, H.F. Xu, T.C. Lowe, Y.T. Zhu, Corrosion resistance of ultra fine-grained Ti, Scripta Materialia 51 (2004) 225–229.
[28] G.R. Argade, S.K. Panigrahi, R.S. Mishra, Effects of grain size on the corrosion resistance of wrought magnesium alloys containing neodymium, Corrosion Science 58 (2012) 145–151.
[29] H.S. Kim, S.J. Yoo, J.W. Ahn, D.H. Kim, W.J. Kim, Ultrafine grained titanium sheets with high strength and high corrosion resistance, Materials Science and Engineering A 528 (29–30) (2011) 8479–8485.